

**Northwest Basin and Range tectonic deformation observed with the Global Positioning
System, 1999-2003**

William C. Hammond¹ and Wayne Thatcher

U.S. Geological Survey, Earthquake Hazards Team

345 Middlefield Rd. MS/977

Menlo Park, CA 94025

¹Now at: Nevada Bureau of Mines and Geology

University of Nevada, Reno

July, 2005

Corresponding author: whammond@unr.edu

Abstract

We use geodetic velocities obtained with the Global Positioning System (GPS) to quantify tectonic deformation of the northwest Basin and Range province of the western United States. The results are based on GPS data collected in 1999 and 2003 across five new quasi-linear networks in northern Nevada, northeast California and southeast Oregon. The velocities show ~ 3 mm/yr westward movement of northern Nevada with respect to stable North America. West of longitude -119° the velocity field is similar to that previously obtained to the south. Velocities increase and turn northwest, parallel to the Sierra Nevada/Great Valley microplate. The observations are explained by a kinematic model with three domains that rotate around Euler poles in eastern Oregon and western Idaho. Northeast California experiences internal dextral shear deformation (11.2 ± 3.6 nanostrains/yr) sub-parallel to Pacific/North America motion. Relative motions of the domains imply 2-5 mm/yr \sim east-west extension in northwest Nevada, and 1-4 mm/yr \sim north-south contraction near the California/Oregon border. The northward-decreasing \sim east-west extension in northwest Nevada is consistent with the northern termination of Basin and Range deformation, faulting and characteristic topography. No significant extension is detected in the Oregon Basin and Range. The Oregon Cascade arc moves north ~ 3.5 mm/yr, and is possibly influenced by the \sim eastward motion of the Juan de Fuca plate. These results disagree with secular northwest trench-ward motion of the Oregon forearc inferred from paleomagnetic rotations. South of latitude 43° , however, trench-ward motion exists, and is consistent with block rotations, \sim east-west Basin and Range extension, and northwest Sierra Nevada translation.

1. Introduction

The northwest Basin and Range province of the interior western United States has experienced distributed continental extension over the past 30 million years. Deformation continues to this day, as evidenced by the many Quaternary and Holocene faults throughout the region [e.g. *Wallace, 1984; Pezzopane and Weldon, 1993; Wesnousky et al., 2004*]. Bounding this part of the province are three tectonic elements that influence its internal deformation. Pacific/North America (PANA) transform motion contributes dextral shear that penetrates at least several hundred kilometers inland, transmitted through the non-deforming Sierra Nevada/Great Valley microplate [*Minster and Jordan, 1984; Flesch et al., 2000*]. The obliquely subducting Juan de Fuca plate causes cyclic, earthquake-related deformation that penetrates central Oregon and Washington [*McCaffrey et al., 2000; Miller et al., 2001; Svarc et al., 2002a*]. To the south and east, broad zones of distributed Basin and Range normal faulting bound our study area.

To date, space geodetic measurement of the northwest part of the province has been sparse. Sampling with the Global Positioning System (GPS) has been limited to a few continuously recording sites in regional networks, with an average station spacing of hundreds of kilometers [*Miller et al., 1998; Wernicke et al., 2000*] or relatively dense measurements at the perimeter of the region [e.g. *Martinez et al., 1998; Thatcher et al., 1999; McCaffrey et al., 2000; Svarc et al., 2002a; Svarc et al., 2002b; Hammond and Thatcher, 2004*]. Several recent analyses have inferred the deformation field by synthesizing and modeling geodetic results across the entire western United States [*Hemphill-Haley and Humphreys, 2000; Flesch et al., 2000; Holt et al., 2003; Kreemer et al., 2003*]. The geodetic results have shown that the vast majority of active deformation occurs in relatively narrow (<200 km wide) belts, which spatially agree very well

with the historical seismic moment release [*Pancha and Anderson, 2004*] and the distribution and repeat frequency of Holocene paleoseismic events [*Wesnowsky et al., 2004*]. Thus, where extension occurs today is a measure of where seismic moment release and surface faulting are likely to occur in future potentially damaging earthquakes.

Here we present results from observation of 86 densely spaced (~20 km) campaign GPS geodetic benchmarks arrayed across the northwest Basin and Range from northern California and central Oregon to easternmost Nevada (Figure 1). Because our networks skirt each of the tectonic provinces that bound this region, our results have kinematic and dynamic implications for Cascadia, the Basin and Range, and the Sierra Nevada/Great Valley microplate.

2. GPS Data

Our network (Figure 1) consists of 86 geodetic benchmarks that span the northwestern part of the Basin and Range province whose positions were measured with temporary occupations of GPS receivers in 1999 and 2003. Twelve additional sites in central Oregon have longer occupation histories (>10 years) and these results have been presented previously by *Svarc et al., [2002a]*. We also obtained data from nearby permanently monumented and continuously recording stations: four sites from the PANGA network [*Miller et al., 1998*] and eight sites from the BARGEN network [*Wernicke et al., 2000*] for each day that we obtained a campaign-mode measurement (Table 1). In total we consider data from 110 geodetic stations. For the campaign-mode sites, we typically collected at least 6.5 hours of data for each of two sessions. However, for approximately 20% of the occupations, between 16 and 24 hours of data was collected per day. Compared to permanently monumented GPS receivers, this mode of surveying allows for a greatly enhanced spatial scope and detail, at the cost of data quantity per

site. We demonstrate below, however, that the uncertainties in site velocity are well determined and small enough to constrain tectonic deformation at the 1-2 mm/yr level.

To infer monument positions we employ precise point positioning [Zumberge *et al.*, 1997] using the GIPSY/OASIS II software version 2.6.1 [Webb and Zumberge, 1995]. Satellite orbit and clock information was obtained from the Jet Propulsion Laboratory. After precise point positioning and ambiguity resolution we applied the Quasi-Observation Combination Analysis (QOCA) filtering algorithm [Dong *et al.*, 1998] to reduce common mode noise arising in the daily realization of the reference frame (version 124 obtained in 2001, see, <http://sideshow.jpl.nasa.gov/~dong/qoca/>). QOCA provides site velocities and their uncertainties using a Kalman filter approach that assumes each station has a velocity that is constant over time. A more complete account of our data processing strategy and method for estimating GPS velocity uncertainty are provided in Hammond and Thatcher, [2004]. There we describe a procedure to scale the velocity uncertainties so that they match the velocity variance after removal of a uniform strain rate model. This is based on the assumption that the variance in residual velocity is an upper limit on intrinsic velocity uncertainty. We repeat that procedure here, and find that the velocity uncertainties are correctly scaled, requiring no further adjustment. The mean east and north velocity uncertainties are 1.3 mm/yr. Of the sites with occupations only in 1999 and 2003 the one standard deviation uncertainties are typically 1.5 and 1.4 mm/yr in the north and east components respectively.

Velocities are provided with respect to fixed North America based on the most recent version of the International Terrestrial Reference Frame (ITRF2000 [Altamimi *et al.*, 2002]). Before specifying the frame we first use a non-fiducial strategy to solve for the positions of sites in our network plus 51 sites in the global tracking network, 13 of which lie on stable North

America. We then transform each of our daily solutions with a coordinate rotation, translation and scale into the reference frame with minimum velocity for sites on the nominally non-deforming part of North America. We obtain this reference frame by rotating ITRF2000 using the Euler pole for North America motion with respect to ITRF2000 (*Altamimi et al.*, [2002], longitude -83.144° , latitude -5.036 , $\omega=0.194^\circ/\text{my}$). This approach uses the strength of the global tracking network to constrain the rotation. Mean velocity magnitude with respect to North America for the four easternmost sites of our network is 3.8 ± 1.4 mm/yr (Figure 2). This is consistent with other GPS measurements that indicate that the eastern Basin and Range moves roughly 3-4 mm/yr with respect to stable North America, and that a velocity gradient of 2-3 mm/yr exists across its eastern boundary, near the Wasatch front [*Martinez et al.*, 1998; *Thatcher et al.*, 1999; *Bennett et al.*, 2003].

3. Deformation Analysis

The GPS velocities exhibit a pattern that strongly suggests rotation around an axis that pierces the surface of the Earth not far from the center of our network (Figure 1). Velocities in northern Nevada trend west, increasing in magnitude and rotating clockwise to the west. At the northern limit of our network, in central Oregon, the velocities are further rotated clockwise and are directed just east of north. Regional long wavelength variations in the magnitudes and trends of the velocities across sub-networks, however, require greater kinematic complexity than can be explained by a single plate rotating around a pole in eastern Oregon.

3.1 Interseismic Strain Accumulation East of the Cascades

Our objective in this study is to relate strain patterns to active faulting, i.e. permanent deformation that occurs over times much greater than the Cascadia megathrust earthquake recurrence interval. Therefore, we subtract from our GPS results model velocities for Cascadia

interseismic accumulation before solving for the best kinematic model. We use the locking parameters from the model of *Svarc et al.*, [2002a] which predict, similar to the models of *Flück et al.*, [1997] and *McCaffrey et al.*, [2000], an east-west contraction, with a velocity gradient of ~ 1 mm/yr. This model was obtained using GPS data broadly distributed over the Oregon and Washington coast ranges and Cascades to characterize shallow locking (i.e. a no slip condition) on a two-plane plate boundary thrust fault, superimposed on rotation of the Oregon coast microplate around a pole of rotation in eastern Oregon. The Cascadia interseismic contraction occurs in the opposite sense of deformation due to Basin and Range normal faulting, which involves east-west extension. Although our network lies east of the zone of locking between the Juan de Fuca and North American plates, and east of the area of strongest interseismic deformation due to the convergence, we find a minimum principal strain rate of -4.6 ± 1.6 nanostrains per year (nstr/yr, negative strains indicate contraction, uncertainty is one standard deviation) oriented $N97^\circ E$ for our sites north of 40° north latitude. The greatest changes in velocities due to this correction are small, ~ 1 mm/yr, and have little effect on the direction of movement of the region covered by our network. However, since the model strain field was obtained using similar GPS data (although of a broader scope) it is not surprising that making the correction removes all of the significant deformation we can detect in the CSOR block. In addition to interseismic strain accumulation and rotation, *Svarc et al.*, [2002a] found a uniform strain rate that amounted to horizontal contraction and shear. We do not detect this additional deformation since their Cascadia megathrust interseismic model can explain all the east-west contraction we observe.

3.2 Three Blocks

We choose a “microplate” approach in order to identify patterns of deformation that are required by the GPS observations. This approach is analytically conservative in that we find a kinematic model having the minimum number of free parameters necessary to explain the data. Relative motions between blocks imply deformation near their boundaries. The method also allows us to distinguish velocity gradients owing to solid body rotation from those that describe deformation. We use the pattern of GPS velocities in Figure 3 to infer the existence of three distinct geodetic domains. These domains consist of contiguous non-overlapping subsets of the surveyed benchmarks. The term “domain” is used because they are allowed to deform with a uniform horizontal tensor strain rate when indicated by the GPS data. However, in some cases no deformation is detected and we will refer to the region as a “block”. Polygons drawn around the domains are for clarity only, and do not necessarily imply a lack of internal deformation (e.g. Figure 3). We denote them as follows: 1) NECA, northeast California, 2) NNV, northern Nevada, and 3) CSOR, central and southern Oregon (Table 3).

To identify the portions of our network that behave rigidly, we initially solve for the tensor strain rate in a large number of overlapping subsets of 10-15 sites. For each subnetwork we perform a least-squares inversion using the relations of *Savage et al.*, [2001] to simultaneously solve for three Euler pole rotation parameters (latitude, λ , longitude, ϕ and rotation rate, ω), and three strain rate parameters $\epsilon_{\theta\theta}$, $\epsilon_{\phi\phi}$, and $\epsilon_{\theta\phi}$ that are estimates of the areal two-dimensional tensor strain rate on a sphere. We find the largest possible set of GPS sites whose relative velocities imply no significant internal deformation by iteratively selecting successively larger groups, stopping before the strain rate parameters becomes significant. At each iteration we inspect the residual velocities of the rest of the network in an attempt to identify systematic differences. The result is our preferred model of three blocks (Figure 3). In

northeast California, significant deformation remains after removing solid-body rotation, and the boundary of this domain is defined by the boundary of the adjacent rigid blocks.

Prior to inferring Euler pole and deformation parameters from the GPS velocities, we remove 6 outliers from the velocities shown in Figure 1 (sites 94FM, CAMU, KMNW, LCCM, PUMP, WALT). Removal is based on the criterion that benchmarks moving approximately normal to the regional velocity pattern represent larger than normal GPS signal noise or local deformation anomalies not representative of the broad-scale tectonics of the northwest Basin and Range. Some vectors that exhibit significant deviation from the regional pattern do not exceed this exclusion criterion, and thus remain in the analysis. However, removing any single vector from the analysis has very little effect on the final result. Velocity outliers are roughly four times as common in this analysis as in the 10 year dataset of *Hammond and Thatcher* [2004] because many sites have only two days of observation in each of 1999 and 2003, and a single daily position outlier will significantly contaminate the inferred velocity. For this reason we did not consider sites for which only a single daily solution was available in a given year, since this makes position outliers impossible to detect and causes underestimation of velocity uncertainties. Additionally, surface deformation owing to fault slip, volcanic activity or human-induced subsidence can locally perturb the regional tectonic signal. For example, between our sites PUMP and VALM, subsidence is occurring owing to water removal related to mining activities that has been independently identified with Interferometric Synthetic Aperture Radar (InSAR) [J. Bell unpublished data]. Our results show that the site PUMP moves in an eastward direction, consistent with its location on the west edge of the subsidence identified by InSAR imaging, and opposite to the regional pattern shown by the other GPS vectors. VALM moves west at an elevated rate compared to nearby sites, consistent with its location on the east side of the

subsidence region. Furthermore, velocities near the Medicine Lake volcanic complex have been omitted from this study because of local deformation from its crustal magmatic system [e.g. *Dzurisin et al.*, 2002].

Multiple Euler poles are needed to describe the transition between the Basin and Range and Cascadia subduction zone. The three domains shown in Figure 3 are necessary and sufficient in number to explain the GPS velocities. Fewer domains result in significantly worse misfit between the kinematic model and the velocities. Using a greater number of domains, or allowing deformation in NNV or CSOR results in data fits that are statistically no better. We performed *F*-tests using the method described by *Stein and Gordon*, [1984] to determine if the reduced misfit owing to increasing the number of domains resulted in a significant improvement in fit or was merely attributable to fewer degrees of freedom in the model (Table 2). The method also allows for a single additional parameter associated with the boundary between domains. Each model was tested against each of the other models. For example, model 7 compared to models 1 through 6 has *F*-test values greater than the *F*-critical values at the 99% confidence level (Table 2). Models 8 and 9 have *F*-test values that are not greater than the *F* critical values, indicating that the additional deformation parameters are not required to explain the GPS velocities. It is important to note that while the error ellipses in Figure 3 overlap in map view, the NECA rotation rate is nearly twice as large and hence is a significantly different Euler vector than those for NNV and CSOR. Furthermore, models where CSOR and NNV blocks have the same Euler pole fit the data significantly worse than models having separate poles (Table 2, model 8: $\chi^2/dof = 1.039$). These models are significantly different to better than 99% confidence when applying the *F*-test criteria of *Stein and Gordon*, [1984].

In our analysis we used data from all the BARGEN sites within the footprint of our network, taking data for each day we had a campaign measurement. However, if we use the published BARGEN velocities of *Bennett et al.*, [2003] in combination with our campaign GPS results instead of the velocities we obtain for those sites, the inferred deformation patterns are unchanged. The *Bennett et al.* [2003] velocities have much smaller uncertainties, as low as 0.06 mm/yr in the north component, since they used daily solutions spanning several years. However, because of differences in reference frame between their results and ours we applied a rotation operator to their velocities to bring them into the same reference frame. After augmenting the uncertainty in the BARGEN velocities with the uncertainty in the reference frame rotation operator, we repeated our analysis. Only minor changes in the Euler poles and strain values are found for the NECA block as a result of using these velocities. For the results shown here we use our own velocities for the BARGEN sites because they are in the same reference frame and have been treated the same as the campaign data during the GIPSY/OASIS II processing.

4. Discussion

4.1 Cascade Forearc Motion

Oregon Cascade forearc motion has been described by *Wells et al.* [1998] as rotation around an Euler pole that lies near the Oregon/Washington border (45.5°N , -119.6°W , $\omega = -1.3^{\circ}/\text{my}$). This description implies that the forearc translates northward over time, explaining both north-south contraction in the Puget Sound/Olympic peninsula area [*McCrary*, 1996] and Cenozoic paleomagnetic rotations inside the forearc [*Wells et al.*, 1998]. However, because their forearc Euler pole position is considerably north of ours, their model also implies a significant west component of forearc motion that increases to the south. This results in motion that must be accommodated by WNW Basin and Range extension and $\text{N}50^{\circ}\text{W}$ migration of the Sierra

Nevada/Great Valley block. Using a more detailed parameterization of the plate locking interface to account for elastic strain accumulation *Miller et al.* [2001] (using the model of *Fliück et al.* [1997]) and *McCaffrey et al.* [2000] found a forearc Euler pole that is very similar to that of *Wells and Simpson*, [2001], and hence also implies significant westward and northward motion of western Oregon.

Our results are only partially consistent with these observations. In the area of overlap with the region studied by *McCaffrey et al.*, [2000] and *Vollick et al.*, [2003], our velocity pattern is qualitatively similar to theirs. The *Wells and Simpson*, [2001] Euler pole is very similar to, but has a much larger uncertainty than the *McCaffrey et al.*, [2000] pole. Both are significantly different from our CSOR pole. In the northern half of our CSOR block, we find northward motion of the arc, forearc and back-arc amounting to ~ 3.5 mm/yr (Figure 3). Our results are not compatible with the ~ 11 mm/yr of trenchward motion of the forearc (as implied by the *Wells and Simpson*, [2001] pole), that would need to be accommodated between the CSOR block and the trench. Such extension would be greater than any seen in the Basin and Range today [*Bennett et al.*, 2003; *Hammond and Thatcher*, 2004] and would require substantial observable geodetic and geologic deformation. In our study, east-west extension across the Cascade arc, the putative eastern boundary of the Cascade forearc microplate, is not significantly different than zero, even after removal of the expected interseismic strain from Cascadia plate interface locking. Nor can we resolve east-west extension in the Oregon Basin and Range, since the velocity gradients in the CSOR block can be explained by solid body rotations. An implication of rotation around the CSOR pole in southeast Oregon is that trench-directed motion of the forearc is near zero at 44° N latitude, but increases southward and by 41° N latitude is ~ 3 mm/yr. However, the location of our NECA Euler pole does predict a westward component of motion of the Oregon forearc south

of 42.5°N latitude, but the velocity azimuths are significantly more northerly than those predicted by the *Wells and Simpson*, [2001] and *McCaffrey et al.*, [2000] poles.

There are several possible explanations for why our results differ from these earlier studies. First, different models of subduction zone interseismic strain accumulation may have different predictions for deformation in the backarc. The trench-parallel component of these models predicts dextral shear that is contained within 100 km of the trench, and thus will not bias the CSOR rotation pole. The trench-normal component extends further inland, and is sensitive to the dip of the plate interface and plate convergence rate. However, we tested the effect of this by varying the trench normal convergence rate by 20%, and the plate interface dip by 5°, variations that are larger than the uncertainties of these values. None of these perturbations generate significantly different strains in the Oregon Cascade backarc. In particular, making the plate interface dip more steeply by 5° makes the CSOR pole move 0.2° north, which is still inside its 95% confidence (Table 3). Along-strike variability in convergence rate or plate coupling can also affect modeled recoverable strain. Second, the Euler pole uncertainties are significant. A model with three separate Euler poles in southeast Oregon could be devised that is consistent within the 95% confidence uncertainties of both studies. This would require only very minor changes in our Euler pole locations, implying that our model is also marginally consistent with the paleomagnetic rotations. Thirdly, the difference between ours and the *Wells and Simpson*, [2001] pole location could be an indication that deformation over the last 60 million years are not representative of contemporary rigid Cascadia backarc motion. A recent reorganization of local tectonic motions and secular translations might also contribute to the discrepancy.

Near the Oregon/California border the direction of northwest Basin and Range motion with respect to North America changes from essentially away from North America to essentially

towards North America (Figure 4). This change coincides with the transition from a Pacific/North America to Juan de Fuca/North America plate boundary, suggesting that our network is detecting a change in the effects of plate boundary forces on deformation of interior North America. Cascade arc migration is not parallel to small circles around the Pacific/North America or Juan de Fuca/North America poles of rotation (Figure 4). The Oregon backarc and Basin and Range have a component of velocity towards the Euler pole of Pacific rotation with respect to North America. This suggests that the tectonic elements surrounding the Cascade forearc have a net influence towards the PA/NA pole of rotation. If the Juan de Fuca plate buttresses the Pacific Northwest from westward extrusion, rather than allowing for its escape, as suggested by some authors [e.g. *Wells et al.*, 1998; *Hemphill-Haley and Humphreys*, 2000]), then it may only do so north of latitude 43°N.

4.2 The Sierra Nevada To Cascadia Transition

Geodetic observations of the Sierra Nevada/Great Valley microplate relative to stable North America require approximately northwest motion around distant Euler poles [*Argus and Gordon*, 1991; *Dixon et al.*, 2000; *Argus and Gordon*, 2001; *McCaffrey*, 2005]. Our results focus on the northern perimeter of the Sierra Nevada, and help delimit the northern extent of its block-like behavior. Our results indicate N43°W oriented dextral shear of the NECA domain, consistent with a Sierra Nevada/Great Valley microplate translating northwest, past the Basin and Range. Moreover, no obvious steps are convincingly resolved between -200 and 0 km in Figure 2c, so this deformation does not seem to be located on any single fault that lies within NECA, but is distributed over two or more fault zones within this domain. This is similar to other recent campaign GPS results for the northern Walker Lane near latitude 40°N, that show northwest oriented shear distributed over 200 km near Pyramid Lake [*Hammond et al.*, 2004].

However, the station-to-station scatter in velocities along the Lassen profile through NECA is large. Nonetheless, the transition between the shearing zone of NECA and the NNV block is apparent in Figure 2c.,

Our observations near the California/Oregon border are consistent with the Sierra Nevada/Great Valley microplate encountering a southwestern Oregon forearc that is reluctantly escaping to the north. The zone of contraction lies in the vicinity of a transition between active Basin and Range normal faulting to the east and the Klamath Mountains to the west (Figure 5). After removal of NECA shear deformation, northward velocities along the Lassen sub-network (in northeast California, Figure 1) are on average 1-4 mm/yr greater than the velocities of the Klamath sub-network (southern Oregon, Figure 1) to the north, indicating a near north-south contraction between these lines. Since velocities near the Medicine Lake volcanic complex have been omitted we cannot resolve in finer detail where this contraction occurs. However, uplift of the Klamath Mountains and the existence of fold and thrust systems in the northern Great Valley [Unruh *et al.*, 2003] are consistent with this convergence, and with the results of regional modeling of geodetic data [Hemphill-Haley and Humphreys, 2000].

4.3 Motion of the Central Basin and Range: Comparison with Highway 50 GPS Results

Our results are consistent with those of another dense geodetic network to the south that has been measured with GPS for 10 years (Figure 4) [Hammond and Thatcher, 2004]. In that network, most of the dextral shear and extension across the Basin and Range is focused near its western perimeter. The eastern part of the province experiences relatively little deformation. If we combine the sites in the non-deforming NNV block of this study and all sites of the Highway 50 network east of the Central Nevada Seismic Belt (CNSB) but west of the Wasatch fault zone (i.e. all sites in the Highway 50 network between longitude 117.8°W and 112.4°W) and solve

simultaneously for deformation and rotation parameters, we find that no internal deformation is required. This group of sites rotates like a solid body around an Euler pole at longitude 116.6°W , latitude 44.5°N , which lies just inside the 95% uncertainty ellipse for the NNV block (Figure 3).

Our Euler pole for the combined eastern Highway 50 and NNV block velocities, located north of the eastern Basin and Range, is very different from the pole found by *McCaffrey* [2005] for approximately the same region. Using a synthesis of geodetic, seismic and geologic data, he placed the pole in the Pacific Ocean off the coast of Baja California. A difference this great cannot be attributed to uncertainty in the fixed North America reference frame. Furthermore, our pole lies inside the two standard deviation uncertainties of the Central Basin and Range pole reported by *Bennett et al.*, [2003] (longitude $92\pm 40^{\circ}\text{W}$, latitude $74\pm 20^{\circ}\text{N}$) but the *McCaffrey* [2005] pole does not. We speculate that the difference between our pole and his might be explained by including smaller GPS velocities near the southern end of the central Basin and Range [R. McCaffrey, personal communication 2005] or by his inclusion of earthquake slip vectors which trend northwest, both of which require a pole to the southwest. Also, we used the more recent GPS results of *Hammond and Thatcher* [2004] which, owing to additional data, resolves more features in the velocity field than does the *Thatcher et al.* [1999] results used by *McCaffrey* [2005].

4.4 Another Central Nevada Seismic Belt?

We have identified a zone of ~east-west extension in northwest Nevada. This zone is the boundary between the NNV and NECA domains, and may be kinematically related to the CNSB, which is a similar band of contemporary near east-west extension. The CNSB is the locus of at least 5 large normal and dextral slip earthquakes (M_w 6.3-7.5) in the 20th century [*Caskey et al.*, 2000], and has been identified geodetically as a zone of anomalously rapid extension [*Hammond*

and Thatcher, 2004], probably enhanced by post-seismic relaxation [Hetland and Hager, 2003]. The zone of extension we infer here is likely west and north of the CNSB (Figure 5), but its width and location are not well constrained by our data.

To test the ability the data have to resolve the boundary between NECA and NNV, we allowed the longitude of the boundary to vary, computing for each longitude the misfit to the GPS velocity data. We tested models where both, none, and just one of the domains were allowed to deform. These tests revealed the following properties of the velocity field: 1) territory east of -120° is not required to deform by the data, 2) if the boundary between the blocks is between -120° and -119° then neither NECA or NNV are required to deform, 3) if only NECA is allowed to deform, then the data are violated if the boundary is west of -120° . Therefore, the east domain deforms only if it includes sites west of -120° , implying the existence of a boundary at -120° . In summary, a clear distinction exists between the velocities east and west of -120° longitude, but the true boundary between blocks could exist as far east as -116° , and could be distributed evenly or be narrowly focused within this zone (Figure 5).

There are several similarities between this zone of extension and the CNSB. They both have similar rates and orientation of extension. They are both west of the Paleozoic continental margin defined by Sr isotopic ratios (Figure 1), and hence are both relatively recent additions to western North America lithosphere. Both are close to the eastern boundary of the Walker Lane, which accommodates nearly all of the contemporary Basin and Range geodetic deformation and has the highest occurrence rates of paleo-earthquakes [Wesnousky *et al.*, 2004]. There is also a significant difference: the CNSB exhibits high rates of present-day crustal seismicity compared to the rest of the Basin and Range, yet our zone of extension in northwest Nevada does not. The southern end of our inferred zone of extension (Figure 5) is near the latitude of the northern end

of the CNSB. However, the relative motion between NECA and NNV implies ~ 5 mm/yr of extension, which is greater than the total velocity gradient across the CNSB. Hence our inferred zone of extension is not simply a northern extension of the CNSB. Also, the NECA and NNV Euler poles likely do not describe relative motion between the eastern Basin and Range and the Walker Lane south of latitude 40°N since this would imply a southward increasing extension rate of >5 mm/yr, which is significantly greater than other recent GPS results show [e.g. *Svarc et al.*, 2002b; *Hammond and Thatcher*, 2004]. Nonetheless, the extension shown in Figure 5 is consistent with indications that the dilatation and shear that overlap at 39° latitude in the Walker Lane, bifurcates to the north into a western zone of dextral shear (in NE California) and an eastern zone of roughly east-west extension (in NW Nevada). How much of this extension can be attributed to a northern extension of the CNSB cannot be resolved with available GPS data.

5. Conclusions

We have used campaign GPS measurements obtained in 1999 and 2003 in southern Oregon, northeast California and northern Nevada to infer deformation patterns in the northwest Basin and Range province of the western United States. GPS velocities show ~ 3 mm/yr of westward movement of northernmost Nevada with respect to North America. West of longitude 119°W the velocities increase and are directed northwest, consistent with approximately northwest movement of the Sierra Nevada microplate beneath the west end of our network, and consistent with previous GPS results across networks to the south.

The GPS data can be explained with a kinematic model having three domains, only one of which need deform. All three rotate around significantly different Euler poles that are located in southeast Oregon or southwest Idaho. Additionally, northeast California deforms in dextral shear (11.2 ± 3.6 nstr/yr) that is parallel to the direction of Sierra Nevada/Great Valley microplate

motion. Rotation of the northeast California domain occurs at a rate nearly twice as large as the Oregon and Nevada blocks, implying a zone of ~north-south directed contraction near the Oregon/California border, and a zone of ~east-west extension in northwest Nevada.

The central Oregon Cascades near latitude 44° north move north with respect to stable North America even after adjustment for the effects of elastic strain accumulation on the Cascadia subduction zone. A lack of measurable extension in the Oregon Basin and Range places a kinematic limit on the allowable amount of trench-ward secular motion of the Oregon Cascade forearc north of latitude 43°N. South of latitude 43°N, however, a trench-ward component of motion does exist and is consistent with gravitationally induced extension of North America.

6. Acknowledgements

We are grateful for the hard work of those who collected data for this investigation: Gerald Bawden, Henry van den Bedem, Elliot Endo, Scott Haefner, Chris Harpel, Marleen Nyst, Mike Poland, Fred Pollitz, Chuck Stiffler, Jim Sutton, and Chuck Wicks. Seth Stein contributed some suggestions on our analysis of microplate significance. We also thank Jim Savage, Mary-Lou Zoback, Rob McCaffrey, Ray Wells and Kelin Wang for their insightful and helpful comments that greatly improved this manuscript.

Table 1. GPS Velocities and Occupation Statistics.

Station	Latitude	Longitude	North America				Corr	ITRF2000		Obs. Days	Time Span (yrs)
			V _N	V _E	σ_N	σ_E		V _N	V _E		
0047	43.59	-119.98	1.2	-2.8	1.3	1.2	-0.06	-11.7	-16.0	5	4.9
1JUN	42.09	-119.66	1.5	-3.3	1.4	1.3	-0.05	-11.3	-16.3	4	3.8
6FMK	41.22	-116.71	-0.3	-2.7	1.2	1.1	0.00	-12.2	-15.9	5	3.8
7MIR	43.17	-120.69	2.7	-0.2	1.5	1.3	0.00	-10.4	-13.2	4	3.8
94FM*	42.86	-117.56	-4.2	-1.1	1.5	1.3	-0.03	-16.4	-14.6	4	3.8
ADIN	41.18	-120.95	8.1	-5.2	1.5	1.5	-0.02	-5.1	-17.8	4	3.8
ALKA	41.55	-120.02	3.8	-3.2	1.5	1.4	-0.05	-9.1	-16.0	6	3.9
ALTU	41.51	-120.50	5.5	-3.7	1.5	1.6	-0.10	-7.5	-16.4	7	3.9
AMOS	41.40	-117.83	0.7	-2.4	1.5	1.4	-0.06	-11.5	-15.5	4	3.8
B428	41.10	-115.11	-0.7	-1.1	1.5	1.4	-0.07	-12.1	-14.5	4	3.8
BATT	40.61	-116.87	1.2	-2.7	1.1	1.1	0.00	-10.7	-15.8	7	3.8
BEAV	43.13	-121.80	5.3	-1.8	0.9	0.8	-0.05	-8.1	-14.7	10	10.9
BEOW	40.66	-116.42	0.4	-2.4	1.5	1.4	-0.08	-11.4	-15.5	4	3.8
BGCR	41.62	-118.45	0.9	-2.6	1.5	1.4	-0.04	-11.5	-15.7	4	3.8
BLAC	41.45	-118.20	2.3	-2.7	1.5	1.4	-0.03	-10.0	-15.8	4	3.8
BLK4	43.16	-122.46	4.3	0.1	0.9	0.8	-0.03	-9.3	-12.7	10	12.0
BLKF	41.35	-121.89	6.6	-5.4	1.4	1.4	-0.02	-6.9	-17.9	5	2.9
BLMT	42.31	-117.81	1.5	-4.1	1.2	1.1	0.00	-10.7	-17.4	7	3.8
BNKS	40.77	-115.92	0.5	-2.9	1.5	1.4	-0.08	-11.1	-16.1	4	3.8
BR02	44.17	-122.33	6.7	0.4	1.8	1.6	-0.03	-6.9	-12.6	4	4.1
BRAM	41.83	-118.58	1.8	-1.2	1.5	1.4	-0.05	-10.7	-14.3	4	3.8
BROT	43.81	-120.60	2.7	-0.1	0.9	0.9	-0.06	-10.4	-13.3	10	10.9
BURN	42.78	-117.84	0.8	-1.4	0.9	0.9	0.00	-11.4	-14.8	128	4.8
BUTN	41.01	-117.57	0.1	-1.9	1.5	1.3	-0.05	-12.1	-15.0	4	3.8
C753	44.31	-120.62	3.1	0.3	1.6	1.5	0.01	-10.0	-13.0	4	4.1
CAMU*	42.22	-120.22	4.2	4.9	1.4	1.2	-0.04	-8.8	-8.0	4	3.8
CEDR	41.55	-120.26	4.7	-5.1	1.5	1.4	-0.06	-8.3	-17.9	4	3.8
CEME	42.19	-121.79	5.0	-2.4	1.3	1.2	-0.03	-8.4	-15.1	5	3.8
CNBY	41.43	-120.87	4.8	-3.4	1.5	1.6	-0.13	-8.4	-16.1	7	3.9
CRTS	40.66	-115.01	-0.7	-2.6	1.1	1.1	-0.01	-12.0	-15.9	6	3.8
CTNP	41.90	-119.47	1.2	-3.0	1.6	1.3	-0.02	-11.5	-16.0	6	3.8
CUPO	44.19	-122.02	7.1	-1.7	1.4	1.3	-0.04	-6.4	-14.7	8	4.0
DRYX	44.21	-121.09	8.1	2.4	1.4	1.3	-0.03	-5.1	-10.8	5	4.1
ELKO	40.91	-115.82	0.1	-3.7	0.9	0.9	-0.01	-11.5	-17.0	117	5.4
EMIG	42.15	-122.62	4.4	-2.8	1.6	1.6	-0.03	-9.3	-15.3	4	3.8
F067	41.88	-119.05	-0.6	-3.3	1.6	1.7	-0.08	-13.2	-16.3	6	3.8
F091	43.39	-120.54	3.1	0.8	1.5	1.5	-0.08	-10.0	-12.3	4	3.8
FARV	43.59	-122.65	4.8	2.1	1.2	1.1	-0.07	-8.9	-10.7	9	7.1
FRAZ	41.10	-121.29	8.0	-9.8	1.5	1.6	-0.09	-5.3	-22.3	4	3.8
GARL	40.42	-119.36	2.6	-5.1	0.8	0.8	-0.01	-10.1	-17.8	703	7.0
GOLC	40.94	-117.47	0.2	-2.6	1.5	1.4	-0.06	-11.9	-15.7	4	3.8
GOSH	40.64	-114.18	-0.7	-3.6	0.8	0.8	-0.01	-11.8	-17.0	77	6.8

GUAN	42.02	-119.48	1.5	-2.4	1.6	1.6	-0.13	-11.2	-15.4	4	3.8
HELO	40.95	-115.62	-1.9	-2.6	1.6	1.6	-0.12	-13.4	-15.9	4	3.8
HHTT	40.87	-121.74	7.2	-7.8	1.4	1.4	0.01	-6.2	-20.2	5	3.8
HILD	42.25	-121.51	4.6	-1.5	1.5	1.4	-0.04	-8.7	-14.2	4	3.8
HOTC	41.49	-120.70	2.6	-4.0	1.5	1.3	-0.04	-10.5	-16.7	4	3.8
HSTN	44.26	-120.93	3.8	1.8	1.4	1.4	-0.05	-9.4	-11.4	5	4.1
HYAT	42.15	-122.50	6.5	-1.7	1.7	1.8	-0.03	-7.1	-14.3	4	3.8
J288	42.41	-121.35	2.7	-1.2	1.5	1.4	-0.08	-10.6	-14.0	4	3.8
J789	42.87	-121.83	4.2	-0.3	1.6	1.6	-0.08	-9.2	-13.1	4	3.8
JHNS	42.14	-122.24	3.8	-3.7	1.1	1.1	0.00	-9.8	-16.3	5	3.8
JUNI	42.93	-119.93	1.9	-1.7	0.9	0.8	-0.07	-11.0	-14.8	11	10.9
K589	42.12	-119.85	1.0	-1.1	1.6	1.6	-0.13	-11.8	-14.1	4	3.8
KMNW*	42.95	-121.58	-1.7	-8.4	1.7	1.7	-0.05	-15.1	-21.3	4	3.8
L091	43.29	-120.64	2.1	-0.7	1.6	1.3	-0.06	-11.0	-13.8	4	3.8
LCCM*	44.18	-122.18	1.7	5.6	1.9	1.5	-0.02	-11.8	-7.4	4	4.1
LOOP	42.72	-118.99	0.4	-3.1	1.3	1.2	0.00	-12.2	-16.3	4	3.8
LUIE	40.40	-116.86	-1.0	-2.6	0.9	0.9	0.00	-12.9	-15.6	32	4.8
M753	44.40	-120.42	4.0	0.8	1.9	1.6	0.01	-9.0	-12.5	4	4.1
MCAR	41.05	-121.40	4.1	-11.0	1.6	1.7	-0.07	-9.2	-23.5	5	3.8
MDLK	41.73	-119.74	-1.3	-3.6	1.5	1.3	-0.03	-14.1	-16.5	6	3.8
MICK	42.66	-118.42	1.6	-2.8	1.1	1.1	0.00	-10.8	-16.1	8	3.8
MINE	40.15	-116.10	-0.2	-2.7	0.9	0.9	-0.01	-11.9	-15.8	106	5.7
MOOR	41.11	-114.80	-1.8	-2.6	1.6	1.8	-0.12	-13.1	-16.1	4	3.8
N067	41.89	-118.85	3.0	-2.9	1.5	1.3	0.02	-9.5	-16.0	4	3.8
OAKR	43.75	-122.50	4.8	1.3	0.9	0.8	-0.03	-8.8	-11.6	12	10.9
OBSD	41.88	-119.24	1.8	-1.8	1.4	1.2	-0.03	-10.9	-14.8	6	3.8
OREG	42.20	-120.59	2.2	-4.0	1.4	1.3	-0.04	-10.9	-16.9	4	3.8
PARA	41.28	-117.69	1.2	-1.7	1.5	1.3	-0.05	-11.0	-14.8	4	3.8
PARS	42.21	-120.07	3.0	-2.7	1.1	1.1	-0.01	-9.9	-15.6	6	3.8
PEQU	41.06	-114.52	-5.5	-2.2	1.6	1.6	-0.08	-16.7	-15.7	4	3.8
PIBU	44.06	-121.28	2.6	-0.6	0.9	0.9	-0.07	-10.7	-13.7	11	10.9
PINE	42.12	-122.37	3.1	-3.4	1.8	1.5	-0.03	-10.5	-16.0	4	3.8
PITR	40.98	-121.54	10.7	-6.5	1.5	1.5	-0.04	-2.7	-19.0	4	3.8
PL20	42.26	-120.72	3.8	-2.6	1.5	1.4	-0.05	-9.3	-15.5	4	3.8
PRIN	44.30	-120.87	4.0	0.0	1.3	1.2	-0.10	-9.2	-13.2	4	6.0
PUMP*	40.89	-117.28	-0.8	2.4	1.7	1.6	-0.05	-12.9	-10.7	5	3.8
Q133	43.02	-118.12	-1.4	-3.0	1.7	1.6	-0.07	-13.7	-16.4	4	3.8
QUIN	39.97	-120.94	6.9	-9.5	0.9	0.9	0.00	-6.3	-21.9	210	4.7
R090	43.48	-120.12	3.8	-0.2	1.4	1.3	0.00	-9.1	-13.4	5	3.8
REDM	44.26	-121.15	2.5	1.0	0.9	0.9	-0.01	-10.7	-12.2	1271	5.8
RMTN	40.80	-121.94	2.1	-3.9	1.5	1.7	-0.05	-11.4	-16.3	4	3.8
ROCO	42.43	-121.10	1.4	-1.1	1.5	1.4	-0.06	-11.8	-13.9	4	3.8
RODM	43.11	-121.27	1.2	-4.7	1.4	1.2	0.00	-12.1	-17.6	5	3.8
RUBY	40.62	-115.12	-0.7	-3.2	0.9	0.9	0.00	-12.1	-16.5	49	6.8
SANM	44.43	-121.95	3.3	2.0	0.9	0.9	-0.04	-10.2	-11.1	10	7.9
SHIN	40.59	-120.23	3.8	-6.2	0.8	0.8	-0.01	-9.2	-18.8	685	6.9

SILV	43.12	-121.06	2.7	-1.4	0.8	0.8	-0.02	-10.5	-14.4	14	10.8
SIST	44.31	-121.56	3.5	1.1	0.9	0.8	-0.04	-9.9	-12.0	8	10.9
SL20	43.08	-121.48	5.9	-1.1	1.5	1.3	-0.02	-7.4	-14.0	5	3.8
SLVZ	40.89	-114.25	-2.3	-0.5	1.7	1.8	-0.08	-13.4	-14.0	4	3.8
SODH	41.41	-118.02	2.5	-1.7	1.2	1.1	0.00	-9.8	-14.8	6	3.8
SOLD	41.07	-121.56	-2.6	-5.0	1.4	1.4	0.20	-16.0	-17.5	6	3.9
STEA	43.34	-122.74	5.2	-0.2	0.9	0.8	-0.10	-8.5	-12.9	14	10.9
T128	42.93	-117.24	-0.3	-2.5	1.6	1.7	-0.01	-12.4	-16.0	4	3.8
TUFF	42.44	-121.21	1.3	-2.5	1.6	1.6	-0.12	-12.0	-15.3	4	3.8
TUNG	40.40	-118.26	1.5	-4.9	0.8	0.8	0.00	-10.9	-17.7	684	7.0
U067	41.94	-118.68	0.9	-6.5	1.5	1.5	-0.02	-11.6	-19.6	6	3.8
U698	43.17	-118.30	-1.7	-1.4	1.6	1.5	-0.06	-14.1	-14.8	4	3.8
VALM	40.78	-117.11	0.0	-5.9	1.5	1.5	-0.12	-12.0	-19.0	4	3.8
VIDA	44.15	-122.57	4.8	2.1	0.9	0.9	-0.01	-8.9	-10.8	12	11.2
W072	43.01	-120.77	2.4	-2.6	1.3	1.3	-0.03	-10.7	-15.6	5	4.9
W67R	42.19	-120.36	3.1	-3.4	0.8	0.8	-0.04	-9.9	-16.3	8	10.8
W784	42.14	-122.01	3.3	-1.1	1.5	1.4	-0.09	-10.2	-13.7	4	3.8
WALT*	44.08	-122.76	-3.1	6.0	1.7	1.5	-0.02	-16.8	-6.9	4	4.1
WICK	43.68	-121.69	3.6	-0.8	0.8	0.8	-0.04	-9.8	-13.8	12	10.9
WILO	41.21	-116.41	-0.6	-2.1	1.2	1.1	0.00	-12.4	-15.4	6	3.8
Y090	43.43	-120.31	3.3	0.6	1.5	1.4	-0.02	-9.7	-12.6	5	3.8
YBHB	41.73	-122.71	6.3	-2.7	0.9	0.9	-0.01	-7.4	-15.1	274	6.7

* Indicates that this site was identified as an outlier and removed from the strain analysis.

Table 2. Blocks Tested Using F -test Method.

Model Index	Number of Blocks	Domains Allowed to Rotate	Domains Allowed to Deform	P	dof	χ^2/dof
1	1	NECA+CSOR+NNV		3	203	1.7591
2	1	NECA+CSOR+NNV	NECA+CSOR+NNV	6	200	1.3556
3	2	NECA, CSOR+NNV		6	200	1.2626
4	2	NECA+CSOR, NNV		6	200	1.3377
5	2	NECA+NNV, CSOR		6	200	1.5692
6	2	NECA, CSOR+NNV		9	197	1.1929
7	3	NECA, CSOR, NNV		9	197	1.1221
8	3	NECA, CSOR, NNV	NECA	12	194	1.0391
9	3	NECA, CSOR, NNV	NECA, NNV	15	191	1.0498
10	3	NECA, CSOR, NNV	NECA, NNV, CSOR	18	188	1.0589

The number of model parameters, P , comes from 3 rotation parameters for non-deforming domains (blocks), 6 for domains that rotate and deform horizontally.

Number of degrees of freedom, dof , is the number of data minus number of model parameters.

Models below the dotted line are not significantly improved by the additional parameters.

An additional degree of freedom for the domain boundaries has been added for each model pair comparison.

Table 3. Rotation and Deformation Parameters for the Preferred Model

Block Name	Longitude	Latitude	ω ($^{\circ}$ /My)	ϵ_1	ϵ_2	ϵ_{Δ}	ϵ_{xy}	α
CSOR	-118.04 \pm 0.30	44.32 \pm 0.15	0.78 \pm 0.07	-	-	-	-	-
NNV	-116.60 \pm 0.32	43.36 \pm 0.57	0.59 \pm 0.13	-	-	-	-	-
NECA	-118.27 \pm 0.39	43.40 \pm 0.36	1.39 \pm 0.20	12.7 \pm 5.1	-9.7 \pm 5.1	3.0 \pm 7.2	11.2 \pm 3.6	-88.2 \pm 11.8

ϵ_1 and ϵ_2 are the maximum and minimum principal strain rates, respectively

$\epsilon_{\Delta} = \epsilon_1 + \epsilon_2$ is the dilatational (horizontal) strain rate.

$\epsilon_{xy} = \gamma/2 = (\epsilon_1 - \epsilon_2)/2$ is the maximum shear strain rate.

α is the geographic azimuth of the direction of maximum extension ϵ_1

CSOR sites: ADIN, ALKA, ALTU, BLKF, CEDR, CNBY, CTNP, FRAZ, GARL, HHTT, HOTC, MCAR, MDLK, PITR, QUIN, RMTN, SHIN

NNV sites: 6FMK, AMOS, B428, BATT, BEOW, BGCR, BLAC, BNKS, BRAM, BUTN, CRTS, ELKO, GOLC, GOSH, HELO, LUIE, MINE, MOOR, PARA, PEQU, RUBY, SLVZ, SODH, TUNG, VALM, WILO

NECA sites: ADIN, ALKA, ALTU, BLKF, CEDR, CNBY, CTNP, FRAZ, GARL, HHTT, HOTC, MCAR, MDLK, PITR, QUIN, RMTN, SHIN

7. References

- Altamimi, Z., P. Sillard, and C. Boucher, ITRF2000: A new release of the International Terrestrial Reference Frame for earth science applications, *J. Geophys. Res.*, 107 (B10), ETG2-1 - ETG2-19, 2002.
- Argus, D.F., and R.G. Gordon, Current Sierra Nevada-North America motion from very long baseline interferometry; implications for the kinematics of the western United States, *Geology*, 19 (11), 1085-1088, 1991.
- Argus, D.F., and R.G. Gordon, Present tectonic motion across the Coast Ranges and San Andreas fault system in Central California, *Geol. Soc. Am. Bull.*, 113 (12), 1580-1592, 2001.
- Bennett, R.A., B.P. Wernicke, N.A. Niemi, A.M. Friedrich, and J.L. Davis, Contemporary strain rates in the northern Basin and Range province from GPS data, *Tectonics*, 22 (2), 3-1 - 3-31, 2003.
- Burchfiel, B.C., D.S. Cowan, and G.A. Davis, Tectonic overview of the Cordilleran orogen in the western U.S., in *The Cordilleran Orogen: conterminous U.S.: The Geology of North America, Volume G-3, Decade of North American Geology*, eds. B.C. Burchfiel, P.W. Lipman, and M.L. Zoback, pp. 407-480, Geol. Soc. Am., Boulder, 1992.
- Caskey, J.S., J.W. Bell, B.D. Slemmons, and A.R. Ramelli, Historical surface faulting and paleoseismology of the central Nevada seismic belt, in *Geological Society of America Field Guide 2*, eds. D.R. Lageson, S.G. Peters, and M.M. Lahren, pp. 23-44, Boulder, Colorado, 2000.
- Dixon, T.H., M. Miller, F. Farina, H. Wang, and D. Johnson, Present-day motion of the Sierra Nevada block and some tectonic implications for the Basin and Range province, North American Cordillera, *Tectonics*, 19 (1), 1-24, 2000.
- Dong, D., T.A. Herring, and R.W. King, Estimating regional deformation from a combination of space and terrestrial geodetic data, *J. Geodesy*, 72, 200-214, 1998.
- Dzurisin, D., Poland, M. P., Burgmann, R., Steady subsidence of Medicine Lake Volcano, Northern California, revealed by repeated leveling surveys, *J. Geophys. Res.*, 107, (B12), 2002.

- Flesch, L.M., J.A. Haines, and W.E. Holt, Dynamics of the India-European collision zone, *J. Geophys. Res.*, 106 (B8), 16,435-16,460, 2001.
- Flesch, L.M., W.E. Holt, J.A. Haines, and S.-T. Bingming, Dynamics of the Pacific-North America Plate boundary in the western United States, *Science*, 287, 834-836, 2000.
- Flück, P., R.D. Hyndman, and K. Wang, Three-dimensional dislocation model for great earthquakes of the Cascadia subduction zone., *J. Geophys. Res.*, 102, 20,539-20,550, 1997.
- Hammond, W.C., and W. Thatcher, Contemporary tectonic deformation of the Basin and Range province, western United States: 10 years of observation with the Global Positioning System, *J. Geophys. Res.*, 109, 1-21, 2004.
- Hammond, W.C., W. Thatcher, G. Blewitt, Crustal deformation across the Sierra Nevada-northern Walker Lane, Basin and Range transition, western United States measured with GPS, 2000-2004
- Hemphill-Haley, M.A., and E.D. Humphreys, Integration of geologic and geodetic data into kinematic models of contemporary strain in the Pacific Northwest and across the Cascadia subduction zone, in *Great Cascadia earthquake tricentennial*, pp. 55-56, Oregon Department of Geology and Mineral Industries, Seaside, OR, United States, 2000.
- Hetland, E.A., and B.H. Hager, Postseismic relaxation across the Central Nevada Seismic Belt, *J. Geophys. Res.*, 108 (B8), ETG 13-1 - ETG 13-13, 2003.
- Holt, W. E., Kreemer, C., Flesch L.M., Haines J.A., R.A. Bennett, The resolving power of the current state of GPS information in North America: Implications for PBO planning, *Eos Trans. AGU* 84(46), 2002.
- Jones, C. H., J. R. Unruh, L. J. Sonder, The role of gravitational potential energy in active deformation in the southwestern United States, *Nature*, 381, 37-41, 1996.
- Kreemer, C., Holt, W.E., Haines, J.A., An integrated global model of present-day plate motions and plate boundary deformation, *Geophys. J. Int.*, 153(1) 8-34, 2003.
- Martinez, L.J., C.M. Meertens, and R.B. Smith, Rapid deformation rates along the Wasatch fault zone, Utah, from first GPS measurements with implications for earthquake hazard, *Geophys. Res. Lett.*, 25, 567-570, 1998.
- McCaffrey, R., Block kinematics of the Pacific - North America plate boundary in the southwestern US from inversion of GPS, seismological, and geologic data, *J. Geophys. Res.*, submitted, 2005.
- McCaffrey, R., M.D. Long, C. Goldfinger, P.C. Zwick, J.L. Nabelek, C.K. Johnson, and C. Smith, Rotation and plate locking at the southern Cascadia subduction zone, *Geophys. Res. Lett.*, 27 (19), 3117-3120, 2000.
- McCrory, P.A., Tectonic model explaining divergent contraction directions along the Cascadia subduction margin, Washington, *Geology*, 24, 929-932, 1996.
- Miller, M., H. Dragert, E. Endo, J.T. Freymueller, C. Goldfinger, H.M. Kelsey, E.D. Humphreys, D.J. Johnson, J.S. Oldow, A. Qamar, and C.M. Rubin, Precise measurements help gauge Pacific Northwest's earthquake potential, *Eos*, 79 (23), 269-275, 1998.
- Miller, M.M., D.J. Johnson, C.M. Rubin, H. Dragert, K. Wang, A. Qamar, C. Goldfinger, GPS-determination of along-strike variation in Cascadia margin kinematics: Implications for relative plate motion, subduction zone coupling, and permanent deformation, *Tectonics*, 20(2), 161-176, 2001.

- Minster, J.B. and T.H. Jordan, Vector constraints on Quaternary deformation of the western United States east and west of the San Andreas fault, *Eos Trans. AGU* 65 (16), 195, 1984.
- Pancha, A., and J.G. Anderson, Comparison of seismic and geodetic scalar moment rates across the Basin and Range province, *Bull. Seismol. Soc. Am.*, *submitted*, 2004.
- Pezzopane, S.K., R.J. Weldon II, Tectonic role of active faulting in central Oregon, *Tectonics* 12(5), 1140-1169, 1993.
- Savage, J.C., W. Gan, and J.L. Svarc, Strain accumulation and rotation in the Eastern California Shear Zone, *J. Geophys. Res.*, 106 (B10), 21,995-22,007, 2001.
- Stein, S. A., and R.G. Gordon, Statistical tests of additional plate boundaries from plate motion, *Earth and Planet. Sci.*, 69 (2), 401-412, 1984
- Svarc, J.L., J.C. Savage, W.H. Prescott, and M.H. Murray, Strain accumulation and rotation in western Oregon and southwestern Washington, *J. Geophys. Res.*, 107 (B5), 2002a.
- Svarc, J.L., J.C. Savage, W.H. Prescott, and A.R. Ramelli, Strain accumulation and rotation in western Nevada, 1993-2000, *J. Geophys. Res.*, 107 (B5), 10.1029/2001JB000579, 2002b.
- Thatcher, W., G.R. Foulger, B.R. Julian, J.L. Svarc, E. Quilty, and G.W. Bawden, Present-Day Deformation Across the Basin and Range Province, Western United States, *Science*, 283, 1714-1718, 1999.
- Unruh, J., J. Humphrey, A. Barron, Transtensional model for the Sierra Nevada frontal fault system, eastern California, *Geology*, 31(4), 327-330, 2003.
- Vollick, J.J., R. McCaffrey, G.F. Sella, C. Stevens, T. Williams, C. McCaffrey, and B. Walton, Block Interactions in Southern Oregon, Northern California, and Northwestern Nevada, *Eos Trans. AGU*, 84 (46), 2003.
- Wallace, R.E., Patterns and timing of late Quaternary faulting in the Great Basin province and relation to some regional tectonic features, *J. Geophys. Res.*, 89 (B7), 5763-5769, 1984.
- Webb, F.H., and J.F. Zumberge, *An introduction to GIPSY/OASIS-II, JPL D-11088*, Pasadena, 1995.
- Wells, R.E., and R.W. Simpson, Northward migration of the Cascadia forearc in the northwest U.S. and implications for subduction deformation, *Earth Planets Space*, 53, 275-283, 2001.
- Wells, R.E., C.S. Weaver, and R.J. Blakely, Forearc migration in Cascadia and its neotectonic significance, *Geology*, 26 (8), 759-762, 1998.
- Wernicke, B.P., A.M. Friedrich, N.A. Niemi, R.A. Bennett, and J.L. Davis, Dynamics of Plate Boundary Fault Systems from Basin and Range Geodetic Network (BARGEN) and Geologic Data, *GSA Today*, 10 (11), 1-7, 2000.
- Wesnousky, S.G., A.D. Baron, R.W. Briggs, J.S. Caskey, S.J. Kumar, and L. Owen, Paleoseismic transect across the northern Great Basin, USA, *J. Geophys. Res.*, *submitted*, 2004.
- Zumberge, J.F., M.B. Heflin, D.C. Jefferson, M.M. Watkins, and F.H. Webb, Precise point positioning for the efficient and robust analysis of GPS data from large networks., *J. Geophys. Res.*, 102 (B3), 5005-5017, 1997.

Figure Captions

Figure 1. Northwest Basin and Range GPS site locations, names and velocities (red vectors) on western U.S. topography. Blue ellipses are 95% confidence in the site velocity with respect to nominally fixed North America. Blue box in inset (upper right) shows location of region with respect to western U.S. states. The western extent of the Paleozoic passive margin is indicated by the heavy dashed gray line [from *Burchfiel et al.*, 1992]. Two-letter designations show the states of CA, California; ID, Idaho; NV, Nevada; OR, Oregon; UT, Utah.

Figure 2. GPS measured velocity with respect to fixed North America as a function of distance from the Pacific/North America (PANA) Euler pole of rotation (arbitrarily offset to zero at the center of the network). Uncertainty bars indicate two standard deviations. Coordinate system is rotated so that in a) and b) positive velocity is towards the Pacific/North America pole of rotation. In c) and d) positive velocity is parallel to Pacific motion with respect to North America, roughly northwest. Sites are divided into the southern half, a) and c), and northern half, b) and d), with a boundary at 42° north latitude. The Nevada sites east of -118.6° longitude have been included in both halves. Triangles, squares and circles belong to the NECA, NNV, and CSOR groups, respectively (see text). A change in the sign of velocity towards the PANA Euler pole is observed between the northern and southern half of the network.

Figure 3. Euler poles (black asterisks) with 95% confidence ellipses for the three domains (light gray shaded polygons) that best explain the GPS velocities are designated CSOR (Central Southern Oregon), NNV (Northern Nevada) and NECA (Northeast California). Each domain is labeled with its corresponding designation. NNV and CSOR are non-deforming after the Cascadia east-to-west elastic strain accumulation model has been removed. NECA experiences right lateral shear in addition to rotation (strain rate tensor bars are black for extension and gray for contraction). The velocities predicted by these Euler poles and strain rate (heavy gray vectors) are plotted beneath the measured velocities (thin black arrows). Note that because of its very different rotation rate, the NECA pole is significantly different than those of CSOR and NNV (see text). Cascade forearc rotation pole of *Svarc et al.* [2002a] is shown with the five-pointed star.

Figure 4. GPS velocities used to develop the kinematic model (red). GPS velocities from the study and *Hammond and Thatcher* [2004] have been included (blue) and the elastic strain accumulation model for Cascadia strain accumulation has been subtracted from all velocities. Outliers have been removed (see text). Light lines indicate faults (gray are Holocene, cyan are historic) from the USGS Quaternary Fault and Fold Database. Strong gradients in GPS velocity are not observed everywhere that there has been recent faulting. Gray short-dashed line is a small circle around the Pacific/North America Euler pole of rotation [*Argus and Gordon*, 2001] (all such small circles are vertical lines in this projection), while the gray long-dashed line is a small circle around the Juan de Fuca/North America Euler pole [*Miller et al.*, 2001]. Solid gray lines are Pacific, North America and Juan de Fuca plate boundaries.

Figure 5. Implications of the idealized deformation model using the Euler poles of Figure 3. Light red vectors are the GPS velocities with respect to non-deforming North America used to find the Euler poles of rotation (magenta stars) for each block (light green shaded polygons).

Yellow arrow couplet in northeast California shows the orientation of right lateral shear deformation (11.2 ± 3.6 nstr/yr) roughly parallel to the Sierra Nevada/North America relative motion. Blue arrows show the location and orientation of the extension and contraction in northwest Nevada and northern California respectively. Circled white numbers indicate magnitude of relative motion implied by block model in mm/yr. Abbreviations are: CA, California; ID, Idaho; NV Nevada; OR, Oregon; UT, Utah. Dashed gray box in northwest NV shows maximum allowable width of the extensional zone.

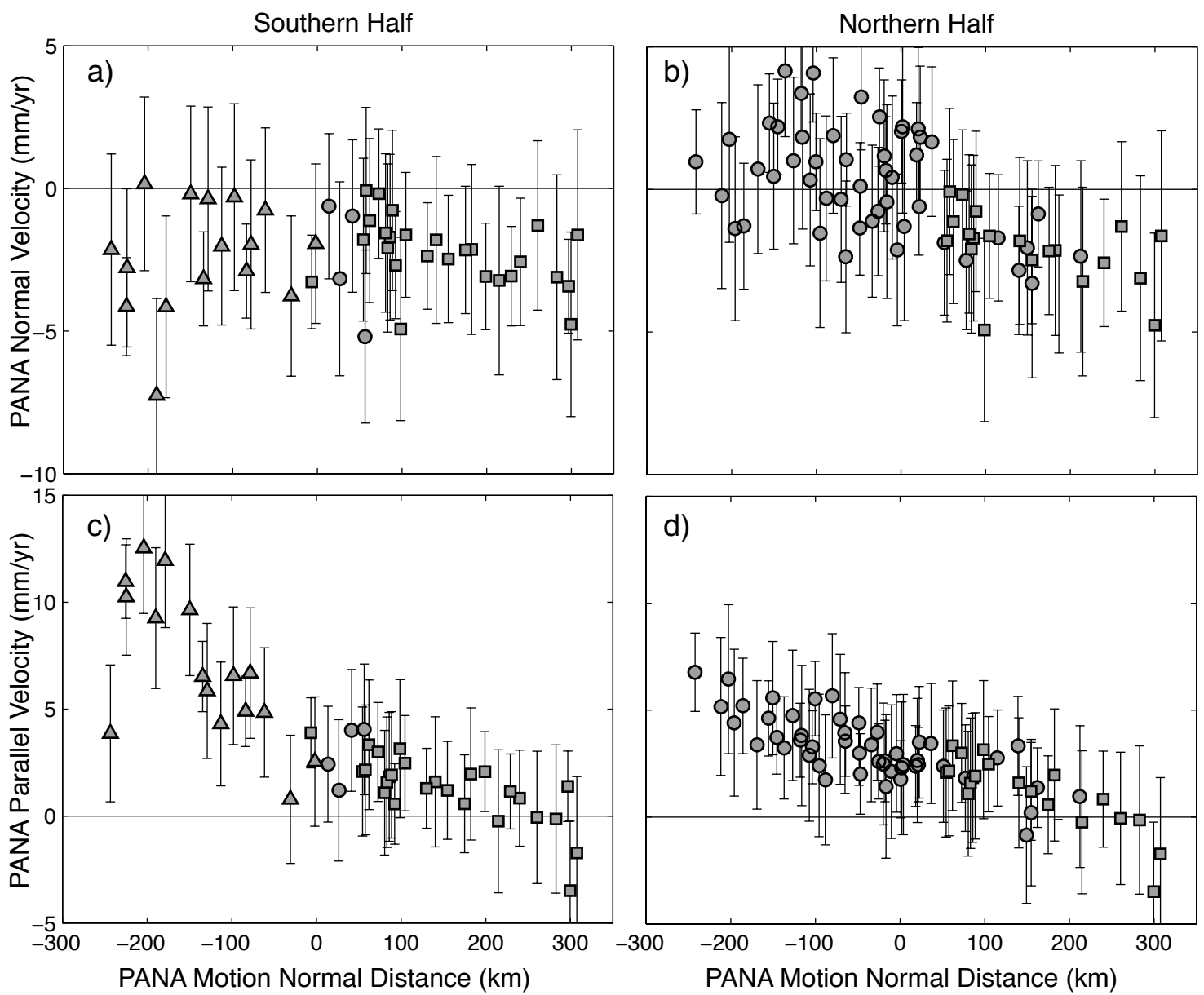


Figure 2: Hammond and Thatcher, 2005

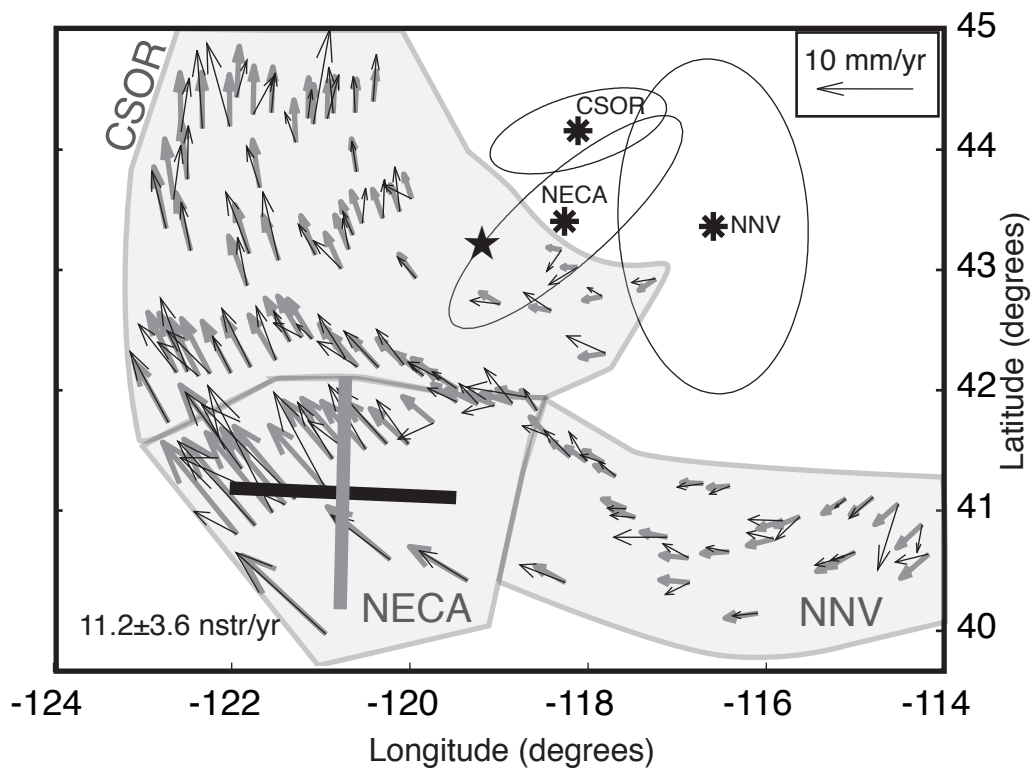


Figure 3: Hammond and Thatcher, 2005

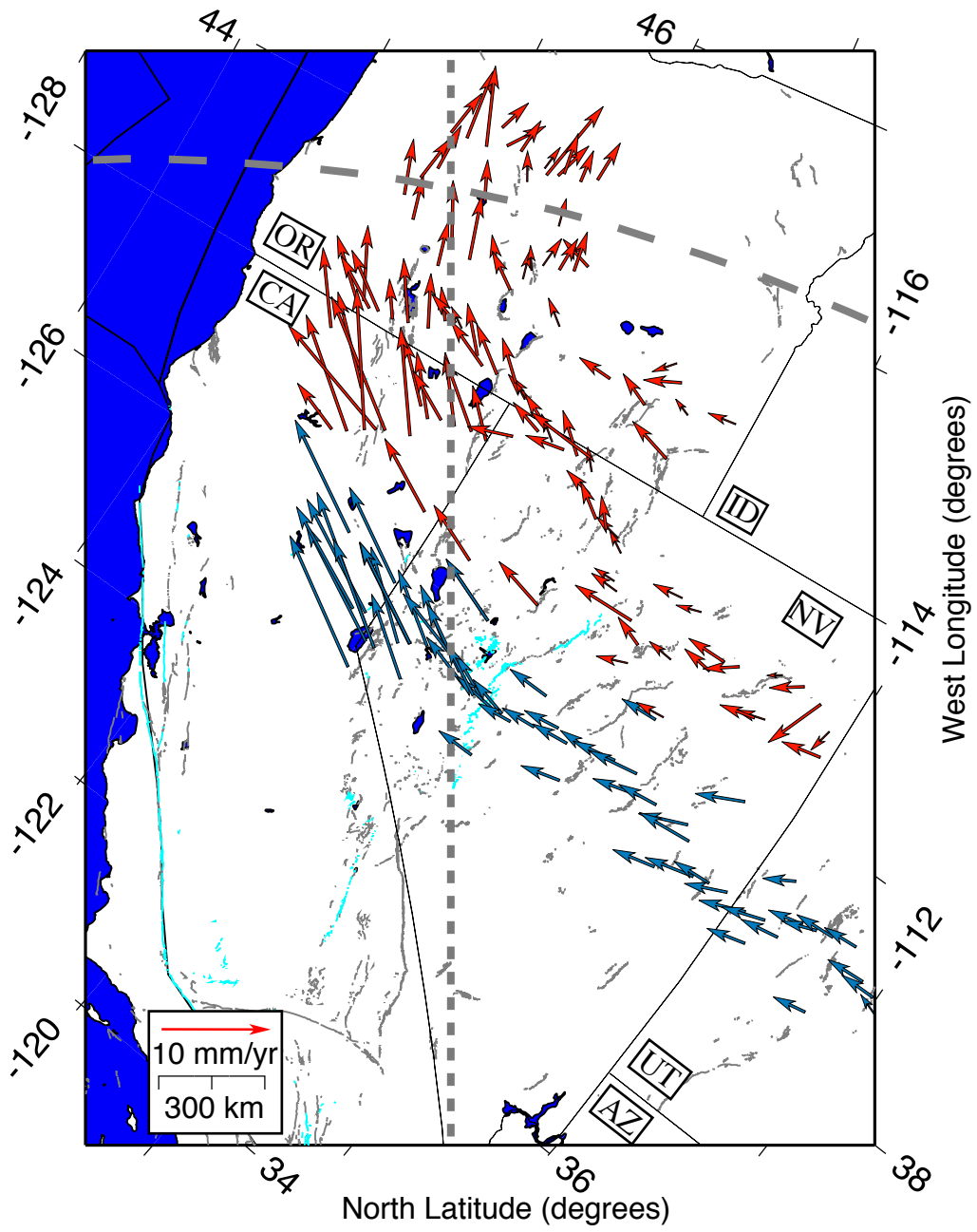


Figure 4: Hammond and Thatcher, 2005

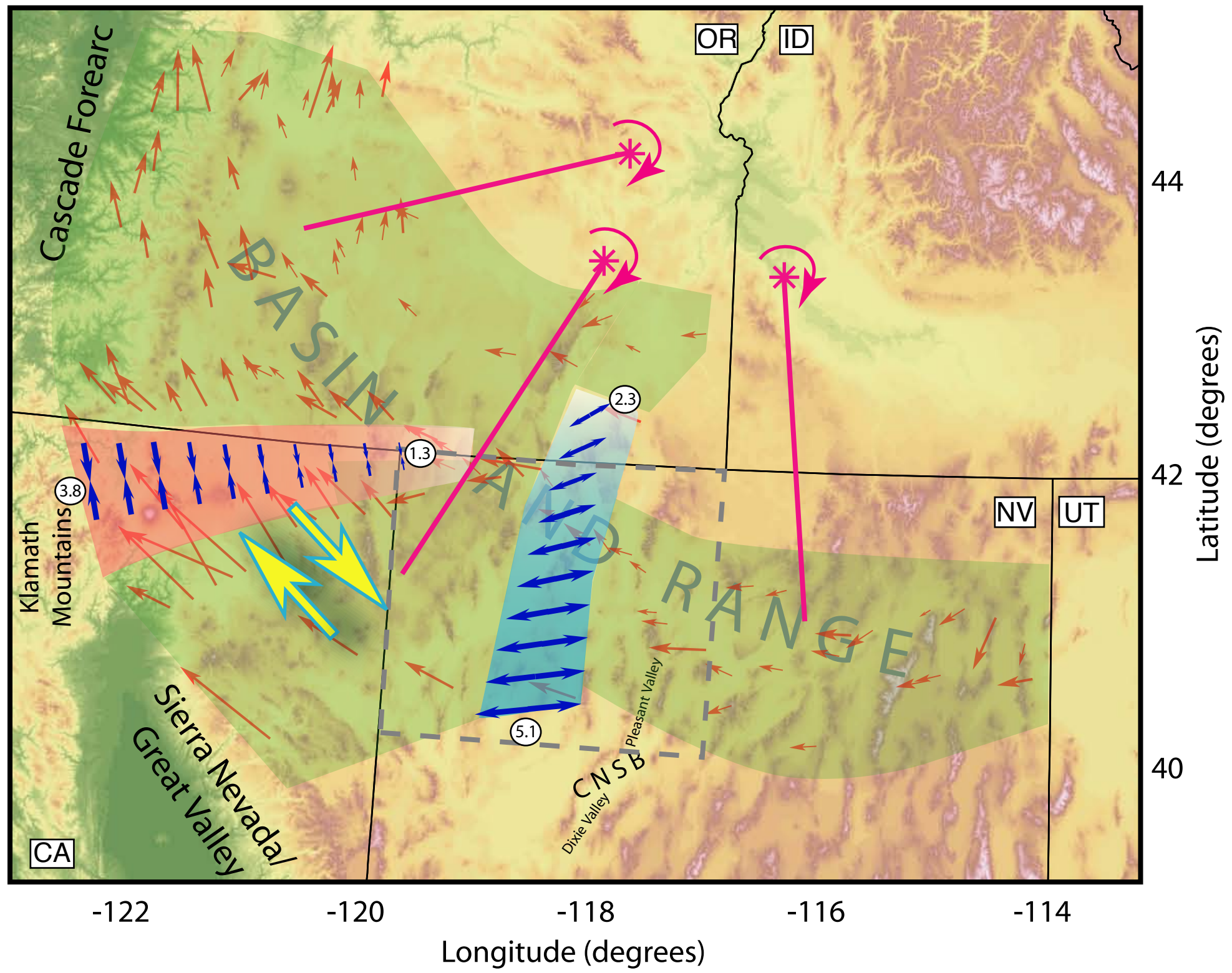


Figure 5: Hammond and Thatcher, 2005